J. Fluid Mech. (1986), *vol.* 164, *pp.* 275–287
Printed in Great Britain

The neutral curve for stationary disturbances in rotating-disk flow

By MUJEEB R. MALIK
High Technology Corporation, P.O. Box 7262, Hampton, Virginia 23666

(Received 25 February 1985 and in revised form 24 September 1985)

The neutral curve for stationary vortex disturbances in rotating-disk flow is computed up to a Reynolds number of 10^7 using the sixth-order system of linear stability equations which includes the effects of streamline curvature and Coriolis force. It is found that the neutral curve has two minima: one at $R = 285.36$ (upper branch) and the other at $R = 440.88$ (lower branch). At large Reynolds numbers, the upper branch tends to Stuart's asymptotic solution while the lower branch tends to a solution that is associated with the wave angle corresponding to the direction of zero mean wall shear.

1. Introduction

The steady flow that exists due to an infinite disk rotating in an otherwise quiescent ambient has been the subject of numerous studies. For this problem, the Navier–Stokes equations reduce to a system of ordinary differential equations but it has been shown (see e.g. Zandbergen & Dijkstra 1977; Lentini & Keller 1980) that the solution is not unique. In the present study, however, we concern ourselves with the stability of the first of these solutions, which is also the classical solution (Cochran 1934) of the von Kármán problem (1921) and is the one observed experimentally in the laminar boundary layer of a rotating disk.

The velocity distribution given by the von Kármán solution is subject to inflexional instability. In their remarkable study using a china-clay technique, Gregory, Stuart & Walker (1955) observed a stationary vortex pattern consisting of about 30 vortices between Reynolds numbers of 430 and 530. Using inviscid theory, Stuart calculated the number of stationary vortices and concluded that the neglect of viscosity gives a number that is almost four times the observed value. However, the predicted wave angle was close to that observed. Later, Brown (1959) and Cebeci & Stewartson (1980), using the Orr–Sommerfeld equation, respectively found that the critical Reynolds numbers were 178 and 176.

Malik, Wilkinson & Orszag (1981) (hereinafter referred to as MWO) considered the effects of Coriolis force, streamline curvature and the radial variation of the mean flow by deriving a sixth-order system of equations, and found the effects to be strongly stabilizing. Wilkinson & Malik (1983), using hot-wire techniques, mapped out the complete wave pattern on the disk and found that the stationary disturbances originate from isolated roughness sites on the disk. Mack (1985) computed the wave pattern observed in the Wilkinson–Malik experiment using the equations of MWO and assuming a white spectrum at the source of the wave pattern.

In the present study, we compute the neutral curve for a disturbance of zero frequency using the equation system of MWO. In §2, we briefly describe the system of equations, while the numerical scheme adopted to solve them is given in §3. Finally, the results are discussed in §4.

2. Analysis

Consider an infinite plane rotating about its axis with angular velocity Ω. We take cylindrical coordinates r^*, θ, z^* with $z^* = 0$ being the plane of the disk and assume the fluid to lie in the half-space $z^* > 0$. Let $\overline{p}$, $\overline{u}$, $\overline{v}$, $\overline{w}$ denote the steady-state values of pressure and velocity in the r^*, θ, z^* directions, respectively, in the rotating coordinate frame. Von Kármán's exact solution of the Navier–Stokes equations for steady laminar rotating-disk flow is obtained by setting

$$\overline{u} = r^*\Omega F(z), \quad \overline{v} = r^*\Omega G(z), \quad \overline{w} = (\nu\Omega)^{\frac{1}{2}} H(z), \quad \overline{p} = \rho\nu\Omega P(z), \tag{2.1}$$

where $z = z^*(\Omega/\nu)^{\frac{1}{2}}$. The Navier–Stokes equations reduce to the following equations for F, G, H and P:

$$F^2 - (G+1)^2 + F'H - F'' = 0; \tag{2.2}$$

$$2F(G+1) + G'H - G'' = 0; \tag{2.3}$$

$$P' + HH' - H'' = 0; \tag{2.4}$$

$$2F + H' = 0; \tag{2.5}$$

where the prime denotes differentiation with respect to z. The boundary conditions are

$$F = 0, \quad G = 0, \quad H = 0 \quad (z = 0), \tag{2.6}$$

$$F = 0, \quad G = -1 \qquad (z \to \infty).$$

Now we study the evolution of infinitesimally small disturbances imposed on the steady flow governed by (2.1)–(2.5). Let r_e^* be the radial location near which the analysis is to be made. Using $r_e^*\Omega$ as the reference velocity, $\delta^* = (\nu/\Omega)^{\frac{1}{2}}$ as the reference length, and $\rho r_e^{*2}\Omega^2$ as the reference pressure, the instantaneous non-dimensional velocities u, v, w and pressure p can be written as

$$u(r,\theta,z,t) = \frac{r}{R}F(z) + \tilde{u}(r,\theta,z,t), \tag{2.7}$$

$$v(r,\theta,z,t) = \frac{r}{R}G(z) + \tilde{v}(r,\theta,z,t), \tag{2.8}$$

$$w(r,\theta,z,t) = \frac{1}{R}H(z) + \tilde{w}(r,\theta,z,t), \tag{2.9}$$

$$p(r,\theta,z,t) = \frac{1}{R^2}P(z) + \tilde{p}(r,\theta,z,t). \tag{2.10}$$

Here the non-dimensional radius is $r = r^*(\Omega/\nu)^{\frac{1}{2}}$, the Reynolds number is

$$R = r_e^*(\Omega/\nu)^{\frac{1}{2}},$$

and r_e^* corresponds to $r = R$.

Substituting (2.7)–(2.10) in the Navier–Stokes equations and linearizing with respect to the perturbations gives

$$\frac{\partial\tilde{u}}{\partial t} + \frac{r}{R}F\frac{\partial\tilde{u}}{\partial r} + \frac{G}{R}\frac{\partial\tilde{u}}{\partial\theta} + \frac{H}{R}\frac{\partial\tilde{u}}{\partial z} + \frac{F}{R}\tilde{u} - \frac{2}{R}(G+1)\tilde{v} + \frac{r}{R}F'\tilde{w}$$
$$= -\frac{\partial\tilde{p}}{\partial r} + \frac{1}{R}\left[\frac{\partial^2\tilde{u}}{\partial r^2} + \frac{1}{r^2}\frac{\partial^2\tilde{u}}{\partial\theta^2} + \frac{\partial^2\tilde{u}}{\partial z^2} + \frac{1}{r}\frac{\partial\tilde{u}}{\partial r} - \frac{2}{r^2}\frac{\partial\tilde{v}}{\partial\theta} - \frac{\tilde{u}}{r^2}\right], \tag{2.11}$$

$$\frac{\partial\tilde{v}}{\partial t}+\frac{r}{R}F\frac{\partial\tilde{v}}{\partial r}+\frac{G}{R}\frac{\partial\tilde{v}}{\partial\theta}+\frac{H}{R}\frac{\partial\tilde{v}}{\partial z}+\frac{F}{R}\tilde{v}+\frac{2}{R}(G+1)\,\tilde{u}+\frac{r}{R}G'\tilde{w}$$
$$=-\frac{1}{r}\frac{\partial\tilde{p}}{\partial\theta}+\frac{1}{R}\left[\frac{\partial^2\tilde{v}}{\partial r^2}+\frac{1}{r^2}\frac{\partial^2\tilde{v}}{\partial\theta^2}+\frac{\partial^2\tilde{v}}{\partial z^2}+\frac{1}{r}\frac{\partial\tilde{v}}{\partial r}+\frac{2}{r^2}\frac{\partial\tilde{u}}{\partial\theta}-\frac{\tilde{v}}{r^2}\right], \quad (2.12)$$

$$\frac{\partial\tilde{w}}{\partial t}+\frac{r}{R}F\frac{\partial\tilde{w}}{\partial r}+\frac{G}{R}\frac{\partial\tilde{w}}{\partial\theta}+\frac{H}{R}\frac{\partial\tilde{w}}{\partial z}+\frac{H'}{R}\tilde{w}=-\frac{\partial\tilde{p}}{\partial z}+\frac{1}{R}\left[\frac{\partial^2\tilde{w}}{\partial r^2}+\frac{1}{r^2}\frac{\partial^2\tilde{w}}{\partial\theta^2}+\frac{\partial^2 w}{\partial z^2}+\frac{1}{r}\frac{\partial\tilde{w}}{\partial r}\right], \quad (2.13)$$

$$\frac{\partial\tilde{u}}{\partial r}+\frac{1}{r}\frac{\partial\tilde{v}}{\partial\theta}+\frac{\partial\tilde{w}}{\partial z}+\frac{\tilde{u}}{r}=0. \quad (2.14)$$

The boundary conditions are that $\tilde{u}$, $\tilde{v}$ and $\tilde{w}$ vanish at $z=0,\infty$.

For $R\gg 1$, (2.11)–(2.14) may be consistently approximated by replacing factors of r by R and neglecting terms of order R^{-2} and smaller. The replacement of r by R at this stage of the calculation implies that we neglect some non-parallel-flow effects. The neglect of terms of order R^{-2} and smaller has little effect on the results discussed below, as we verified by computations in which they were included.

Replacing factors of r by R in (2.11)–(2.14) gives a set of equations that is separable in r, θ, t so that the perturbation quantities may be assumed to have the form

$$(\tilde{u},\tilde{v},\tilde{w},\tilde{p})=(f(z),g(z),h(z),\pi(z))\exp[\mathrm{i}(\alpha r+\beta R\theta-\omega t)]. \quad (2.15)$$

With this assumption, (2.11)–(2.14) become (not yet dropping terms of order R^{-2})

$$\mathrm{i}(\alpha F+\beta G-\omega)f+F'h+\mathrm{i}\alpha\pi=\frac{1}{R}[f''-\lambda^2 f-Ff+2(G+1)g-Hf']$$
$$+\frac{1}{R^2}[\mathrm{i}\alpha f-2\mathrm{i}\beta g]-\frac{1}{R^3}f, \quad (2.16)$$

$$\mathrm{i}(\alpha F+\beta G-\omega)g+G'h+\mathrm{i}\beta\pi=\frac{1}{R}[g''-\lambda^2 g-Fg-2(G+1)f-Hg']$$
$$+\frac{1}{R^2}[\mathrm{i}\alpha g+2\mathrm{i}\beta f]-\frac{1}{R^3}g, \quad (2.17)$$

$$\mathrm{i}(\alpha F+\beta G-\omega)h+\pi'=\frac{1}{R}[h''-\lambda^2 h-Hh'-H'h]+\frac{\mathrm{i}}{R^2}\alpha h, \quad (2.18)$$

$$\left[\mathrm{i}\alpha+\frac{1}{R}\right]f+\mathrm{i}\beta g+h'=0, \quad (2.19)$$

where $\lambda^2=\alpha^2+\beta^2$.

Eliminating π from (2.16)–(2.18) by means of (2.19) gives, neglecting terms of order R^{-2} and smaller,

$$[\mathrm{i}(\mathrm{D}^2-\lambda^2)(\mathrm{D}^2-\bar{\lambda}^2)+R(\alpha F+\beta G-\omega)(\mathrm{D}^2-\bar{\lambda}^2)-R(\bar{\alpha}F''+\beta G'')$$
$$-\mathrm{i}H\mathrm{D}(\mathrm{D}^2-\bar{\lambda}^2)-\mathrm{i}H'(\mathrm{D}^2-\bar{\lambda}^2)-\mathrm{i}F\mathrm{D}^2]h+[2(G+1)\,\mathrm{D}+2G']\eta=0, \quad (2.20)$$

$$[2(G+1)\,\mathrm{D}-\mathrm{i}R(\alpha G'-\beta F')]h+[\mathrm{i}(\mathrm{D}^2-\lambda^2)+R(\alpha F+\beta G-\omega)-\mathrm{i}H\mathrm{D}-\mathrm{i}F]\eta=0, \quad (2.21)$$

where $\mathrm{D}=\mathrm{d}/\mathrm{d}z$, $\bar{\alpha}=\alpha-\mathrm{i}/R$, $\bar{\lambda}^2=\alpha\bar{\alpha}+\beta^2$ and $\eta=\alpha g-\beta f$ is proportional to the z-component of the perturbation vorticity. The final result, (2.20) and (2.21), is a consistent set of stability equations valid to order R^{-1}. Note that, if the Coriolis-force and streamline-curvature effects are neglected, the above system reduces to

the fourth-order Orr–Sommerfeld equation. Equations (2.20) and (2.21) may be represented as a system of first-order equations:

$$\frac{d\phi_i}{dz} = \sum_{j=1}^{6} a_{ij}\phi_j \quad (i = 1, ..., 6), \tag{2.22}$$

where

$$\phi_1 = h, \quad \phi_2 = \frac{d\phi_1}{dz}, \quad \phi_3 = \frac{d\phi_2}{dz},$$

$$\phi_4 = \frac{d\phi_3}{dz}, \quad \phi_5 = \alpha g - \beta f, \quad \phi_6 = \frac{d\phi_5}{dz},$$

and the non-zero elements of the matrix a_{ij} are

$$a_{12} = 1, \quad a_{23} = 1, \quad a_{34} = 1,$$

$$a_{41} = -[\lambda^2\bar{\lambda}^2 + iR(\alpha F + \beta G - \omega)\bar{\lambda}^2 + iR(\bar{\alpha}F'' + \beta G'') + H'\bar{\lambda}^2],$$

$$a_{42} = -H\bar{\lambda}^2, \quad a_{43} = \lambda^2 + \bar{\lambda}^2 + iR(\alpha F + \beta G - \omega) + H' + F,$$

$$a_{44} = H, \quad a_{45} = 2iG', \quad a_{46} = 2i(G+1), \quad a_{56} = 1,$$

$$a_{61} = R(\alpha G' - \beta F'), \quad a_{62} = 2i(G+1),$$

$$a_{65} = \lambda^2 + iR(\alpha F + \beta G - \omega) + F, \quad a_{66} = H.$$

The boundary conditions at the solid boundary are

$$\phi_1(0) = \phi_2(0) = \phi_5(0) = 0. \tag{2.23}$$

The boundary conditions imposed far away from the surface of the disk are derived from the asymptotic form of (2.20) and (2.21) by requiring that all disturbances should decay exponentially. The specific form of these boundary conditions is

$$\phi_4 - \gamma_1\phi_3 - \bar{\lambda}^2\phi_2 + \gamma_1\bar{\lambda}^2\phi_1 = 0, \tag{2.24}$$

$$\phi_4 + [\bar{\lambda}^2 - (\gamma_1 + \gamma_2)]\phi_3 + [\gamma_1\gamma_2 - \bar{\lambda}(\gamma_1 + \gamma_2)]\phi_2 + \bar{\lambda}\gamma_1\gamma_2\phi_1 = 0. \tag{2.25}$$

$$\phi_6 - \gamma_1\phi_5 = 0, \tag{2.26}$$

where

$$\gamma_1 = \tfrac{1}{2}H(\infty) - [(\tfrac{1}{2}H(\infty))^2 + \lambda^2 - iR(\beta + \omega)]^{\frac{1}{2}},$$

$$\gamma_2 = \tfrac{1}{2}H(\infty) + [(\tfrac{1}{2}H(\infty))^2 + \lambda^2 - iR(\beta + \omega)]^{\frac{1}{2}}.$$

3. Numerical method

In order to solve the governing equations, we use a compact fourth-order finite-difference scheme proposed by Malik, Chuang & Hussaini (1982). The scheme is derived by means of the Euler–Maclaurin formula

$$\psi^k - \psi^{k-1} = \tfrac{1}{2}y_k\left(\frac{d\psi^k}{dz} + \frac{d\psi^{k-1}}{dz}\right) - \tfrac{1}{12}y_k^2\left(\frac{d^2\psi^k}{dz^2} - \frac{d^2\psi^{k-1}}{dz^2}\right) + O(y_k^5), \tag{3.1}$$

where

$$\psi^k = \psi(z_k), \quad y_k = z_k - z_{k-1}.$$

In order to resolve singular layers, we consider two different node distributions. First,

$$z_k = \frac{L(k-1)}{Ns - (k-1)} \quad (k = 1, 2, ..., N+1), \tag{3.2}$$

where $N+1$ is the total number of nodes, $s = 1 + L/z_\infty$, z_∞ the location of the far-field boundary, and L a scaling parameter.

Secondly,

$$z_k = \left[1-\cos\left\{\frac{\pi(k-1)}{N_1-1}\right\}\right]^{\frac{1}{2}} L \quad (k = 1, 2, \ldots, N_1), \tag{3.3a}$$

and

$$z_k = L+\left[1-\cos\left\{\frac{\pi(k-N_1)}{2(N-N_1+1)}\right\}\right](z_\infty - L) \quad (k = N_1+1, \ldots, N+1). \tag{3.3b}$$

The results reported in the next section have been obtained using the node distribution (3.2) unless otherwise mentioned. The values of z_∞, L and N are chosen to be 20, 1.8 and 200, respectively.

To apply the above compact-difference scheme to (2.22), we set

$$\psi = \{\phi_i\}, \quad \frac{\mathrm{d}\psi}{\mathrm{d}z} = \left\{\sum_{j=1}^{6} a_{ij}\phi_j\right\}, \quad \frac{\mathrm{d}^2\psi}{\mathrm{d}z^2} = \left\{\sum_{j=1}^{6} b_{ij}\phi_j\right\},$$

where

$$b_{ij} = \frac{\mathrm{d}a_{ij}}{\mathrm{d}z} + \sum_{l=1}^{6} a_{il}a_{lj},$$

and thus (3.1) becomes

$$\phi_i^k - \tfrac{1}{2}y_k \sum_{j=1}^{6} a_{ij}^k \phi_j^k + \tfrac{1}{12}y_k^2 \sum_{j=1}^{6} b_{ij}^k \phi_j^k - \left\{\phi_i^{k-1} + \tfrac{1}{2}y_k \sum_{j=1}^{6} a_{ij}^{k-1}\phi_j^{k-1} + \tfrac{1}{12}y_k^2 \sum_{j=1}^{6} b_{ij}^{k-1}\phi_j^{k-1}\right\} = 0$$
$$(k = 2, 3, \ldots, N+1). \tag{3.4}$$

It is possible to write the above equation system along with the boundary conditions (2.23–2.26) in block-tridiagonal form:

$$\mathbf{L}\boldsymbol{\phi} = \boldsymbol{M}, \tag{3.5}$$

where $\mathbf{L} = [\boldsymbol{A}_k, \boldsymbol{B}_k, \boldsymbol{C}_k]$. Here $\boldsymbol{A}_k$, $\boldsymbol{B}_k$ and $\boldsymbol{C}_k$ are 6×6 matrices and $\boldsymbol{M}$ is a null matrix. Assuming that an estimate of the eigenvalue is available, we solve (3.5) directly. To avoid trivial solution, inhomogeneous boundary conditions are imposed at the wall. Specifically, the boundary condition $\phi_1(0) = 0$ is replaced by $\phi_3(0) = 1$. This is equivalent to normalizing the eigensolution by the value of $\mathrm{d}^2h/\mathrm{d}z^2$ at the wall. As a result, the system (3.5) is inhomogeneous and the non-trivial solution is obtained by using block LU factorization. Newton's method is then used for an iteration on the eigenvalue such that the remaining boundary condition $\phi_1(0) = 0$ is satisfied.

To generate a neutral curve ($\alpha_i = \beta_i = \omega_i = 0$) for a given ω_r, a solution $\boldsymbol{\phi}$ is first obtained for assumed values of α_r and β_r. (We will drop the subscript r in the following discussion.) The corrections $\Delta\alpha$ and $\Delta\beta$ are then determined from the equations

$$\phi_{1r}(0) + \frac{\partial\phi_{1r}(0)}{\partial\alpha}\Delta\alpha + \frac{\partial\phi_{1r}(0)}{\partial\beta}\Delta\beta = 0, \tag{3.6}$$

$$\phi_{1i}(0) + \frac{\partial\phi_{1i}(0)}{\partial\alpha}\Delta\alpha + \frac{\partial\phi_{1i}(0)}{\partial\beta}\Delta\beta = 0. \tag{3.7}$$

Here $\phi_1(0)$ is known from the solution $\boldsymbol{\phi}$ just obtained, while the derivatives with respect to α and β are obtained by solving

$$\mathbf{L}\frac{\partial\boldsymbol{\phi}}{\partial\alpha} = -\frac{\partial\mathbf{L}}{\partial\alpha}\boldsymbol{\phi} \tag{3.8}$$

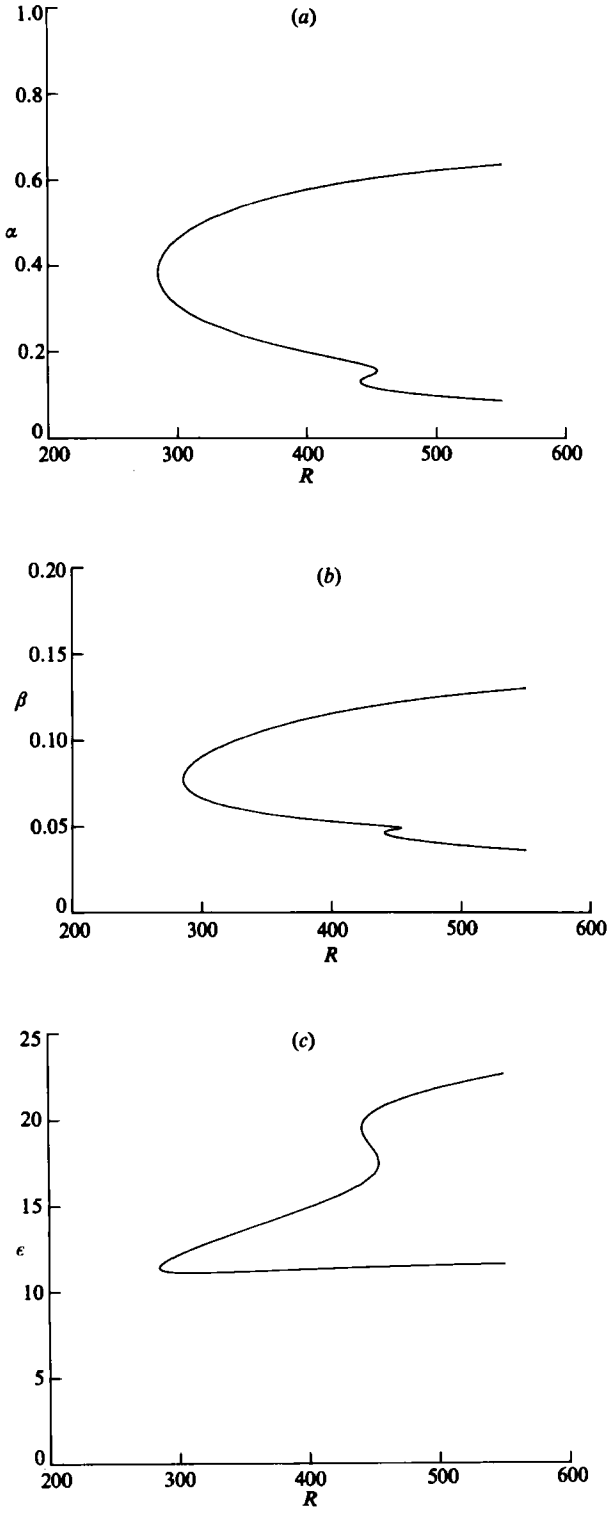

FIGURE 1. Neutral curve for disturbances of zero frequency in rotating-disk flow: (a) (α, R)-plane; (b) (β, R)-plane; (c) (ϵ, R)-plane.

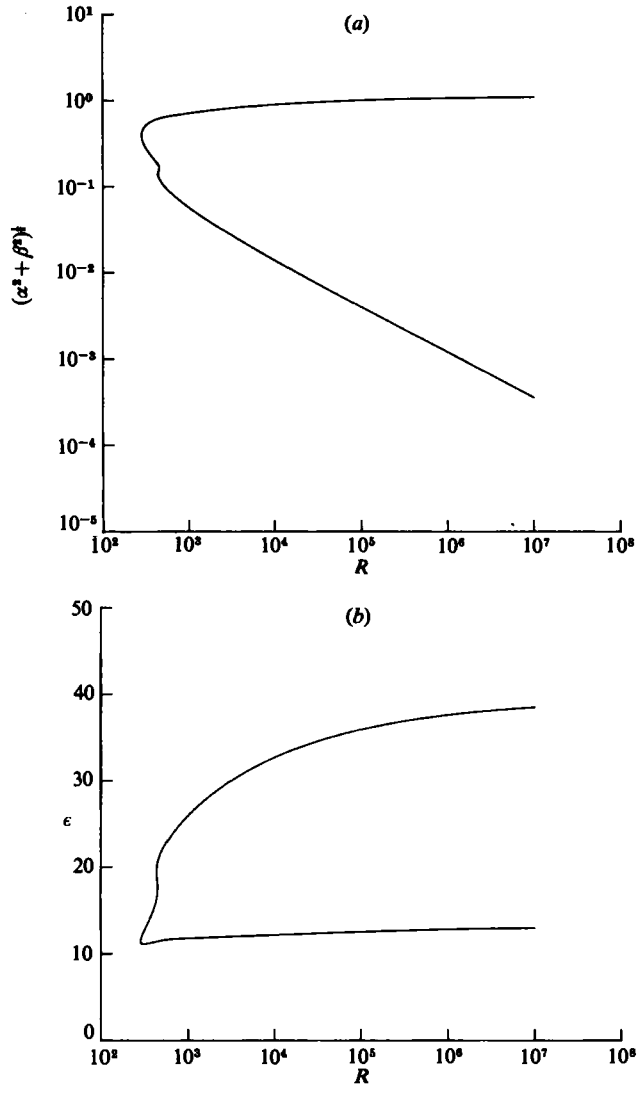

FIGURE 2. Neutral curve for zero-frequency disturbances: (*a*) $(\alpha^2+\beta^2)^{\frac{1}{2}}-R$ plane using log–log scale; (*b*) (ϵ, R)-plane using semi-log scale.

and
$$\mathbf{L}\frac{\partial \boldsymbol{\phi}}{\partial \beta} = -\frac{\partial \mathbf{L}}{\partial \beta}\boldsymbol{\phi}. \tag{3.9}$$

The process is repeated until $\phi_1(0)$ vanishes within preassigned tolerances. We see that (3.5), (3.8) and (3.9) can be solved with the same LU factorization and both the eigenvalue and eigenfunction are obtained.

In the next section we present the results of the stability calculations. The mean flow was obtained by a fourth-order-accurate Runge–Kutta scheme. The computed values of the important mean-flow parameters are $F'(0) = 0.51023$, $G'(0) = -0.61592$ and $H(\infty) = -0.884$.

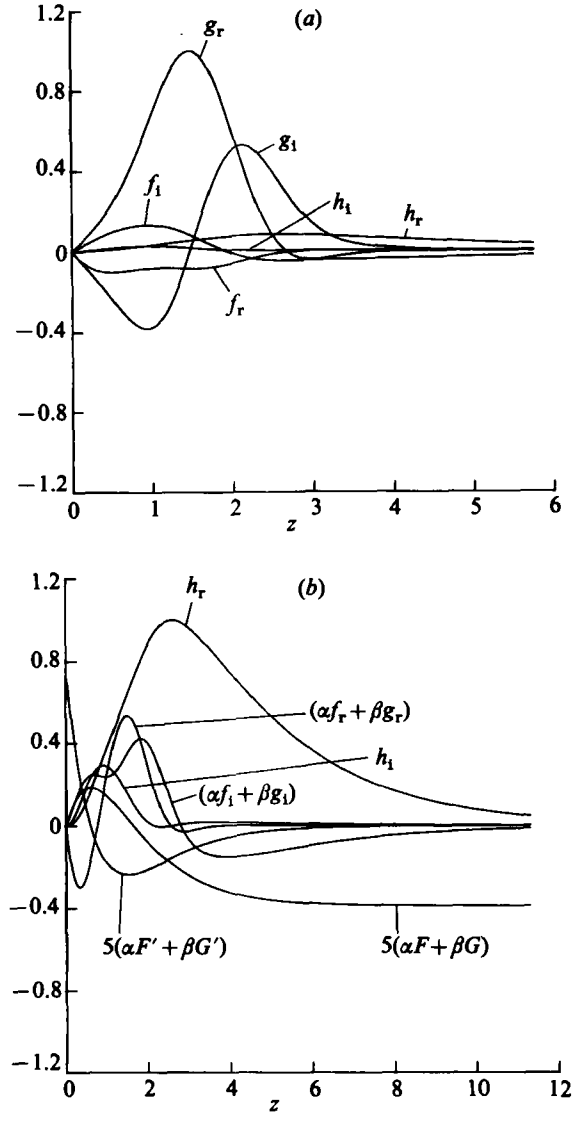

FIGURE 3. Real and imaginary parts of the eigenfunction and mean-flow profile along the upper branch at $R = 285.36$, $\alpha = 0.38482$, $\beta = 0.07759$. (*a*) f, g, h are respectively the radial, azimuthal and vertical (normal to the disk) components of the eigenfunction. These components have been scaled so that the maximum is 1. (*b*) $\alpha F+\beta G$ is the mean flow parallel to the disk in a direction that is at 90° to the vortex axis and $\alpha f+\beta g$ is the eigenfunction in that direction, while h is the eigenfunction in the vertical direction. $\alpha F'+\beta G'$ is the derivative of the mean flow with respect to distance normal to the disk and is proportional to the mean shear stress.

4. Results and discussion

The calculated neutral curves for stationary-disturbance-vortex flow in the (α, R)-, (β, R)- and (ϵ, R)-planes ($\epsilon = \tan^{-1}\beta/\alpha$) are presented in figure 1. The minimum critical Reynolds number is 285.36. This value is more accurately calculated than the value of 287 reported in MWO. The critical parameters are $\alpha = 0.38482$, $\beta = 0.07759$, $\epsilon = 11.4°$. From the evidence provided by the hot-wire measurements of Wilkinson & Malik (1983), Kobayashi, Kohama & Takamadate (1980) and others it can be

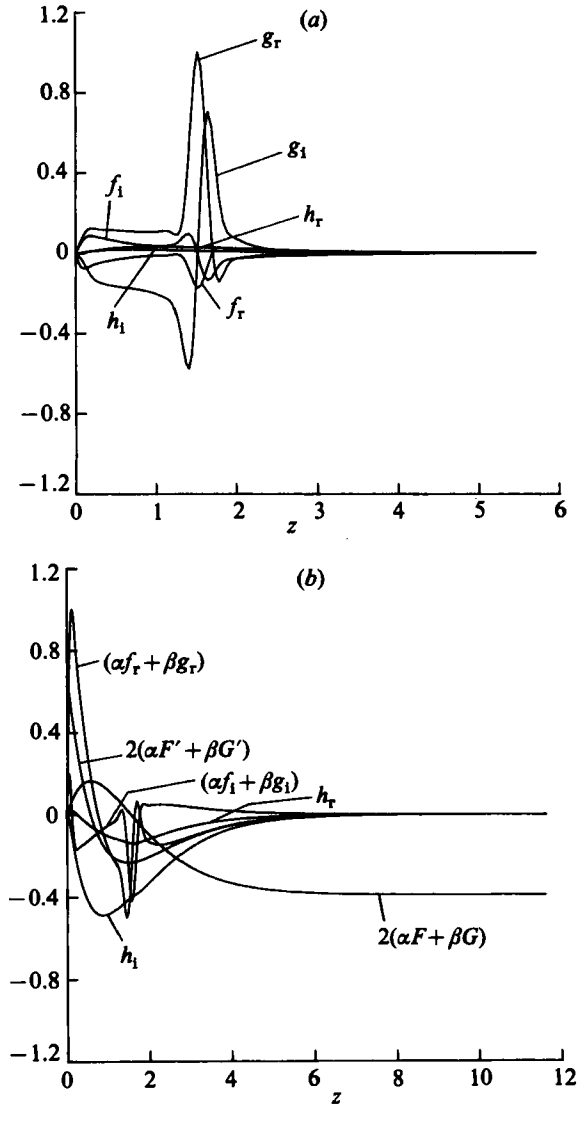

FIGURE 4. Real and imaginary parts of the eigenfunction and mean-flow profile along the upper branch at $R = 15000$, $\alpha = 0.90337$, $\beta = 0.19572$: (*a*) as in figure 3(*a*); (*b*) as in figure 3(*b*).

concluded that the critical Reynolds number for the onset of the stationary-disturbance-vortex flow falls in the range 290 ± 20. The calculated value of 285.36 is then in excellent agreement with the experiment. It should be noted that, if the fourth-order Orr–Sommerfeld equation is solved instead of the system (2.22)–(2.26), the critical Reynolds number is 175 ± 5 (Brown 1959; Cebeci & Stewartson 1980 and MWO), which is well below the observed value.

Wilkinson & Malik (1983) found that the wave angle is in the range 11°–14°. The wave angle of 11.4° at the critical point is therefore within the observed range.

A notable feature of the neutral curves presented in figure 1 is the appearance of a second minimum on the lower branch. This minimum appears at $R = 440.88$ with the critical parameters being $\alpha = 0.13228$, $\beta = 0.04672$, $\epsilon = 19.45°$. The wavenumber

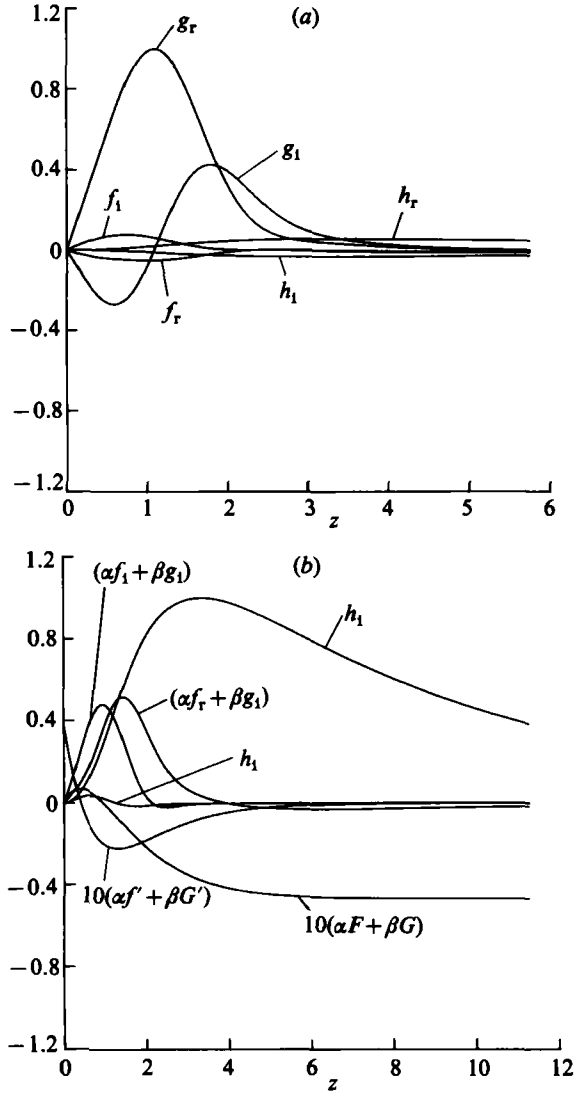

FIGURE 5. Real and imaginary parts of the eigenfunction and mean-flow profile along the lower branch at $R = 440.88$, $\alpha = 0.13228$, $\beta = 0.04672$: (*a*) as in figure 3(*a*); (*b*) as in figure 3(*b*).

and the angle are intriguingly close to the second set of stationary vortices observed in the experiment of Fedorov *et al.* (1976). However, the observed critical Reynolds number for these disturbances was even below the critical Reynolds number 285.36 for the establishment of 30 or so vortices. Mack (1985) also noted the second family of zero-frequency solutions in his computations.

It is interesting to look at the behaviour of the two branches of the neutral curve at large Reynolds numbers. The calculations were performed up to $R = 10^7$ and the results are presented in figure 2. The upper branch tends to the asymptotic solution obtained by Stuart (Gregory *et al.* 1955). The calculated wavenumber $(\alpha^2+\beta^2)^{\frac{1}{2}}$ at $R = 10^7$ is 1.119 and the wave angle is 12.95°. The corresponding inviscid values obtained by Stuart were 1.141 and 13.3°. The wavenumber therefore drops along the upper neutral curve from 1.141 at the inviscid limit to 0.392 at the critical point, while

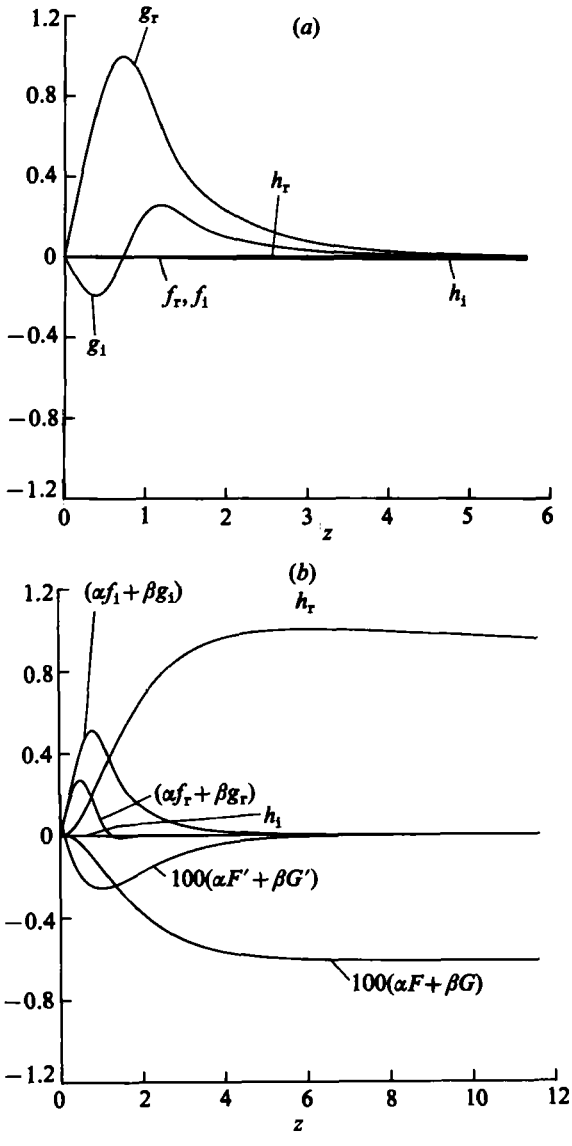

FIGURE 6. Real and imaginary parts of the eigenfunction and mean-flow profile along the lower branch at $R = 15000$, $\alpha = 0.00929$, $\beta = 0.00614$: (*a*) as in figure 3(*a*); (*b*) as in figure 3(*b*).

the wave angle only changes from 13.3° to 11.4°. So the original claim by Stuart that viscosity has large effect on wavenumber is confirmed. The eigenfunctions at $R = 285.36$ and $R = 15000$ along the upper branch are plotted in figures 3 and 4, respectively. Both figures have two parts: in part (*a*) f, g and h are plotted such that the maximum value of g is 1; and in part (*b*) $\alpha f+\beta g$ and h are plotted normalized with the maximum value. In part (*b*) of the figures, the mean-flow quantities $\alpha F+\beta G$ and $\alpha F'+\beta G'$ are also plotted. It is clear that the critical layer is located in the boundary layer where $\alpha F+\beta G = 0$.

Along the lower branch at large Reynolds number, $\log(\alpha^2+\beta^2)^{\frac{1}{2}}$ behaves like $\log R^{\chi}$ where $\chi \simeq -0.53$. The wave angle continuously increases along this branch from

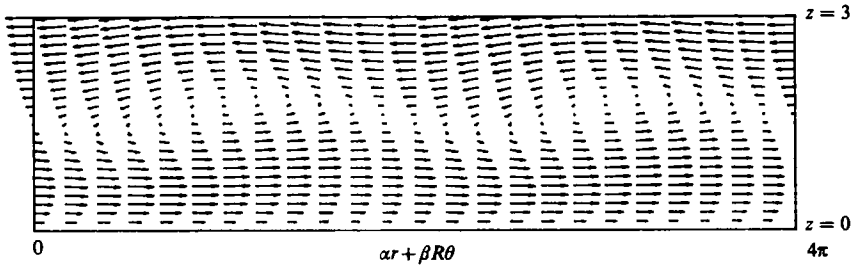

FIGURE 7. Velocity-vector plot showing the structure of stationary disturbance vortices at the flow conditions of figure 3. The actual (physical) view can be obtained by stretching the horizontal axis three times and keeping the vertical axis unchanged.

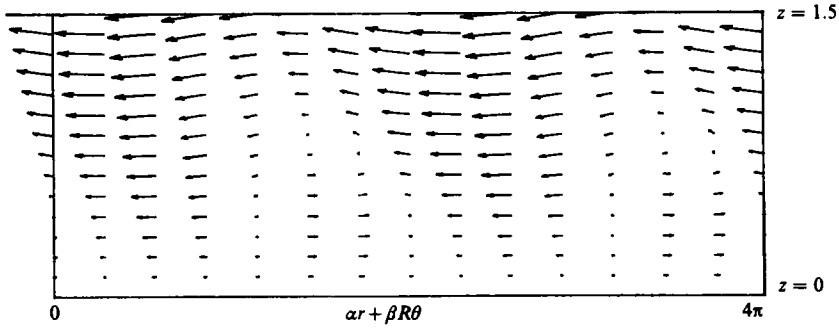

FIGURE 8. Velocity-vector plot showing the structure of stationary disturbance vortices at the flow conditions of figure 6. The actual (physical) view can be obtained by stretching the horizontal axis 300 times and keeping the vertical axis unchanged.

$\epsilon = 19.45$ at $R = 440.88$ to $\epsilon = 38.54$ at $R = 10^7$. At $R = 10^7$, $\alpha = 0.2841 \times 10^{-3}$ and $\beta = 0.2263 \times 10^{-3}$. The wave angle appears to be tending to $\epsilon = 39.64°$; i.e. the direction of zero wall mean shear stress. The eigenfunctions at two Reynolds numbers ($R = 440.88$ and $R = 15000$) along the lower branch are plotted in figures 5 and 6. It can be discerned from these figures that wall mean shear stress decreases with Reynolds number along the lower branch while the opposite is true along the upper branch. The calculations along the lower branch for $R > 10^5$ were performed using the node distribution (3.3) with $N_1 = \frac{1}{3}N$ and $L = 0.5$.

The computed stationary-vortex structure is presented in figure 7. The figure contains the vector plot of velocity components

$$[\alpha F + \beta G + a\,\mathrm{Re}\{(\alpha f + \beta g)\,E\}] \quad \text{and} \quad \left[\frac{H}{R} + a\,\mathrm{Re}\{hE\}\right],$$

where $E = \exp[\mathrm{i}(\alpha r + \beta R\theta)]$. The amplitude a was taken to be 0.2 and the eigenfunctions were from the calculation made at the critical Reynolds number, $R = 285.36$. The centre of these vortices is located at about $z = 1.8$, i.e. at 36 % of the boundary-layer thickness. Contrary to the suggestion of Stuart (see Gregory *et al.* 1955), only one set of vortices is present. It is possible that the second set, which could be nearest the wall, will have been obliterated by viscosity. It was shown by Wilkinson & Malik (1983) that the stationary disturbances originate from isolated roughness sites on the disk and the familiar 30 or so vortex pattern emerges only when the different wave packets have spread and filled the entire disk circumference. It has been made clear

by the calculations of Mack (1985) that what is observed in the experiment is the result of the superposition of the complete zero-frequency azimuthal wavenumber spectrum.

It will be interesting to see the vortex structure along the lower branch of the neutral curve. We present such a plot in figure 8, where the vortex structure is shown for $R = 15000$. The centre of these long-wavelength vortices is located at about $z = 0.7$ and it moves closer to the wall as the Reynolds number is increased. The trend is opposite along the upper branch. It should be noted that the scale in figures 7 and 8 was chosen to give the best visual picture. In order to get an idea of the actual length of the vortices with respect to distance normal to the disk, the horizontal axis should be stretched three times in figure 7 and 300 times in figure 8.

This work was sponsored by NASA Langley Research Center under Contract No. NAS1-16916.

REFERENCES

Brown, W. E. 1959 *Northrop Report* NAI-59-5.

Cebeci, T. & Stewartson, K. 1980 *AIAA J.* **18**, 1485.

Cochran, W. G. 1934 *Proc. Camb. Phil. Soc.* **30**, 365.

Fedorov, B. I., Plavnik, G. Z., Prokhorov, I. V. & Zhukhovitskii, L. G. 1976 *J. Engng Phys.* **31**, 1448.

Gregory, N., Stuart, J. T. & Walker, W. S. 1955 *Phil. Trans. R. Soc. Lond.* A **248**, 155.

Kármán, Th. von 1921 *Z. angew. Math. Mech.* **1**, 232.

Kobayashi, R., Kohama, Y. & Takamadate, Ch. 1980 *Acta Mechanica* **35**, 71.

Lentini, M. & Keller, H. B. 1980 *SIAM J. Appl. Maths* **38**, 52.

Mack, L. 1985 *AIAA Paper No.* 85-0490.

Malik, M. R., Chuang, S. & Hussaini, M. Y. 1982 *Z. angew. Math. Phys.* **33**, 189.

Malik, M. R., Wilkinson, S. P. & Orszag, S. A. 1981 *AIAA J.* **19**, 1131.

Wilkinson, S. P. & Malik, M. R. 1983 *AIAA Paper No.* 83-1760. (Also *AIAA J.* **23** (1985), p. 588.)

Zandbergen, P. J. & Dijkstra, D. 1977 *J. Engng Maths* **11**, 167.